Artificial Fusion of mCherry Enhances Trehalose Transferase Solubility and Stability

Mestrom, Luuk; Marsden, Stefan R.; Dieters, Marit; Achterberg, Puck; Stolk, Lysanne; Bento, Isabel; Hanefeld, Ulf; Hagedoorn, Peter Leon

DOI
10.1128/AEM.03084-18

Publication date
2019

Document Version
Final published version

Published in
Applied and Environmental Microbiology

AMERICAN SOCIETY FOR MICROBIOLOGY | Applied and Environmental Microbiology®

ENZYMOLOGY AND PROTEIN ENGINEERING

Artificial Fusion of mCherry Enhances Trehalose Transferase Solubility and Stability

Luuk Mestrom,[a] Stefan R. Marsden,[a] Marit Dieters,[a] Puck Achterberg,[a] Lysanne Stolk,[a] Isabel Bento,[b] Ulf Hanefeld,[a] Peter-Leon Hagedoorn[a]

[a]Biocatalysis, Department of Biotechnology, Delft University of Technology, Delft, The Netherlands
[b]EMBL Hamburg, Hamburg, Germany

ABSTRACT LeLoir glycosyltransferases are important biocatalysts for the production of glycosidic bonds in natural products, chiral building blocks, and pharmaceuticals. Trehalose transferase (TreT) is of particular interest since it catalyzes the stereo- and enantioselective α,α-(1→1) coupling of a nucleotide sugar donor and monosaccharide acceptor for the synthesis of disaccharide derivatives. Heterologously expressed thermophilic trehalose transferases were found to be intrinsically aggregation prone and are mainly expressed as catalytically active inclusion bodies in *Escherichia coli*. To disfavor protein aggregation, the thermostable protein mCherry was explored as a fluorescent protein tag. The fusion of mCherry to trehalose transferase from *Pyrobaculum yellowstonensis* (*Py*TreT) demonstrated increased protein solubility. Chaotropic agents like guanidine or the divalent cations Mn(II), Ca(II), and Mg(II) enhanced the enzyme activity of the fusion protein. The thermodynamic equilibrium constant, K_{eq}, for the reversible synthesis of trehalose from glucose and a nucleotide sugar was determined in both the synthesis and hydrolysis directions utilizing UDP-glucose and ADP-glucose, respectively. UDP-glucose was shown to achieve higher conversions than ADP-glucose, highlighting the importance of the choice of nucleotide sugars for LeLoir glycosyltransferases under thermodynamic control.

IMPORTANCE The heterologous expression of proteins in *Escherichia coli* is of great relevance for their functional and structural characterization and applications. However, the formation of insoluble inclusion bodies is observed in approximately 70% of all cases, and the subsequent effects can range from reduced soluble protein yields to a complete failure of the expression system. Here, we present an efficient methodology for the production and analysis of a thermostable, aggregation-prone trehalose transferase (TreT) from *Pyrobaculum yellowstonensis* via its fusion with mCherry as a thermostable fluorescent protein tag. This fusion strategy allowed for increased enzyme stability and solubility and could be applied to other (thermostable) proteins, allowing rapid visualization and quantification of the mCherry-fused protein of interest. Finally, we have demonstrated that the enzymatic synthesis of trehalose from glucose and a nucleotide sugar is reversible by approaching the thermodynamic equilibrium in both the synthesis and hydrolysis directions. Our results show that uridine establishes an equilibrium constant which is more in favor of the product trehalose than when adenosine is employed as the nucleotide under identical conditions. The influence of different nucleotides on the reaction can be generalized for all LeLoir glycosyltransferases under thermodynamic control as the position of the equilibrium depends solely on the reaction conditions and is not affected by the nature of the catalyst.

KEYWORDS glycosyltransferase, protein solubility, trehalose transferase, inclusion bodies, mCherry, protein aggregation

Citation Mestrom L, Marsden SR, Dieters M, Achterberg P, Stolk L, Bento I, Hanefeld U, Hagedoorn P-L. 2019. Artificial fusion of mCherry enhances trehalose transferase solubility and stability. Appl Environ Microbiol 85:e03084-18. https://doi.org/10.1128/AEM.03084-18.

Editor Maia Kivisaar, University of Tartu

Address correspondence to Peter-Leon Hagedoorn, P.L.Hagedoorn@tudelft.nl.

Received 24 December 2018
Accepted 1 February 2019
Accepted manuscript posted online 8 February 2019
Published 4 April 2019

Trehalose [α-D-glucopyranosyl-(1→1)-α-D-glucopyranoside] is a nonreducing disaccharide with an α,α-glycosidic linkage that has been identified in plants, insects, fungi, bacteria, and archaea (1–5). The functional role of trehalose as an intracellular osmolyte is to manage the cell volume during exposure to intra- or extracellular osmotic, thermal, and oxidative stresses. Trehalose is a nonionic kosmotrope which preserves the protein hydration shell by reducing the water activity, a_w (6). Moreover, during anhydrobiosis trehalose protects the cell membranes by direct binding to phospholipids, preventing water leakage during rehydration (7). Due to the absence of a free aldehyde moiety, trehalose is highly resistant to heat and changes in pH and does not degrade via the Maillard reaction (8). Unsurprisingly, trehalose is commonly found in extremophiles which have to withstand harsh growth conditions such as extreme temperatures, high ionic strengths, and acidic or basic environments (1).

Several metabolic pathways for the biosynthesis of trehalose have been found in nature (Fig. 1) and include the following: (i) trehalose synthase (TreS) interconverting maltose to trehalose (9); (ii) maltooligosyltrehalose synthase (TreYZ) hydrolyzing maltodextrins to trehalose (10, 11); (iii) inverting trehalose phosphorylase ($TreP_{inv}$) (12–15) adding α-D-glucose-1-phosphate or (iv) retaining trehalose phosphorylase ($TreP_{ret}$) (16–19) adding β-D-glucose-1-phosphate to glucose, producing trehalose and phosphate; (v) trehalose transferase (TreT) using D-glucose and a nucleotide diphosphate (NDP) sugar to produce D-trehalose (20–25); (vi) trehalose phosphate synthase (OtsA) producing D-trehalose-6-phosphate from D-glucose-6-phosphate and a nucleotide sugar (26–30). In contrast to trehalose phosphate synthase, the LeLoir glycosyltransferase TreT does not require the use of additional 6-phosphate (OtsA), avoiding sequential dephosphorylation of the nonreducing disaccharides, and therefore is of particular interest for industrial food applications (31, 32). Additionally, the selective coupling of sugar donors and unprotected monosaccharide acceptors to nonreducing carbohydrates cannot be achieved by chemical catalysts, while glycosyl hydrolases and transferases enable the transfer of sugar acceptors in a regio-, enantio-, and stereospecific manner (33).

TreT from *Thermoproteus tenax* (*Tt*TreT) has previously been applied in enzymatic sugar coupling for the production of nonnatural trehalose derivatives, but the variation of sugar acceptors was limited (34). Currently, the main limitations for biotechnological applications of TreT are the low protein stability, solubility, and formation of inclusion bodies (IBs) during heterologous expression in *Escherichia coli* (21). The formation of inclusion bodies is reported for 70% of all recombinant proteins (35), constituting one of the major obstacles for heterologous expression systems that emphasizes the requirement for solubility tags. Despite these challenges, trehalose transferase has been recognized for its high total turnover number during catalysis (20, 33). The aim of this study was to create a stable, robust trehalose transferase expression system for the enzymatic synthesis of trehalose derivatives. Since protein folding and aggregation are governed by hydrophobic and electrostatic interactions, the aggregation-prone behavior of several homologous trehalose transferases, with different pI values, from hyperthermophilic *Crenarchaeota* was investigated in order to address this issue. For this purpose, the TreT proteins from *Pyrobaculum yellowstonensis* WP-30 (*Py*TreT), *Thermoproteus tenax* Kra1 (*Tt*TreT), and *Thermoproteus uzoniensis* 768-20 (*Tu*TreT) were selected.

Additionally, the fluorescent protein mCherry was fused to *Py*TreT as a direct reporter for promoting protein solubility. In addition to a short maturation time and an excellent photostability of the chromophore, the fluorescent protein possesses the required thermostable properties to match its fusion partner. While the complete mechanisms behind protein aggregation and the formation of inclusion bodies remain elusive, the fusion of fluorescent proteins to aggregation-prone enzymes to monitor protein solubility has previously been successfully applied for a variety of enzymes (36–39). The use of a fusion complex has remained largely limited to the visualization of proteins *in vivo* rather than enzyme catalysis *in vitro*. In this study, we explored the use of mCherry fusion to the aggregation-prone trehalose transferase as a solubility

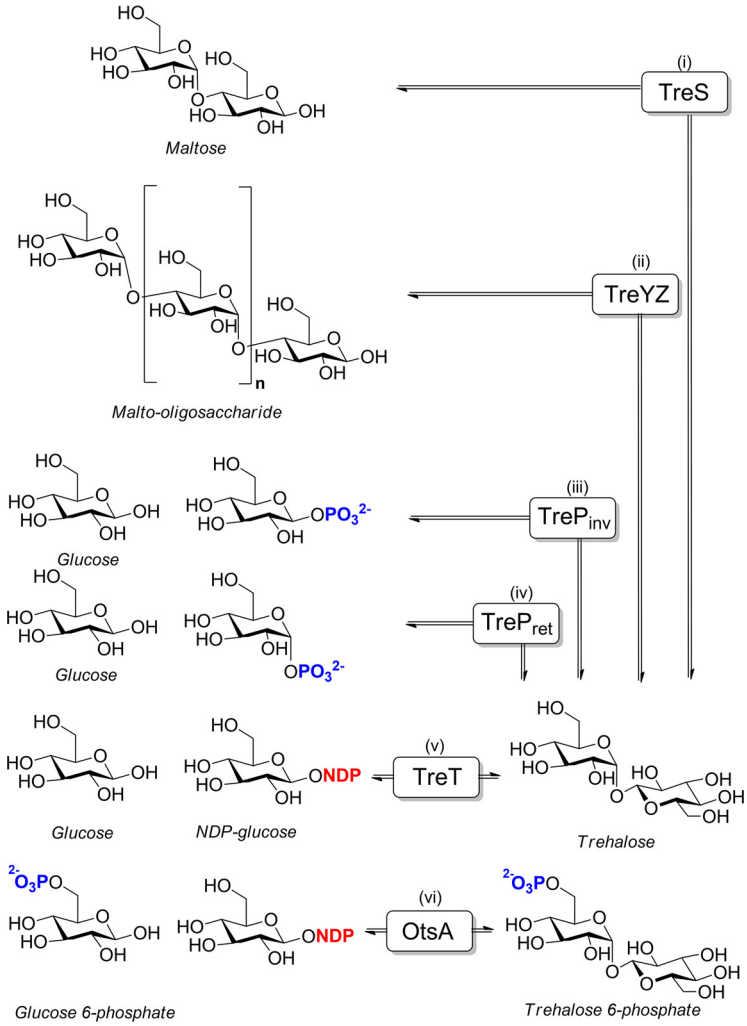

FIG 1 Biosynthesis of trehalose using trehalose isomerase (TreS), trehalose hydrolase/isomerase (TreYZ), inverting ($TreP_{inv}$) and retaining ($TreP_{ret}$) phosphorylases, trehalose transferase (TreT), and trehalose phosphate synthase (OtsA).

enhancement tag to address the challenging recombinant expression of archaeal glycosyltransferases.

RESULTS

Recombinant expression of TreT. Recombinant expression of *Tt*TreT from the pET302 plasmid in *E. coli* BL21(DE3) was previously reported to lead to the formation of insoluble inclusion bodies (IBs) (21). Therefore, *Tt*TreT was expressed using the pBAD/His A plasmid in *E. coli* Top10 based on previous results, where the formation of insoluble inclusion bodies was not reported (40). The protein solubility of TreT was evaluated in the expression host *E. coli* Top10 in parallel expression experiments using the pBAD/His A vector harboring an empty plasmid or the genes encoding *Tt*TreT, *Tu*TreT, or *Py*TreT. The cells were harvested, lysed, and evaluated in terms of protein content, purity, and activity. High overexpression of TreT was observed in all cases, but the enzymes were predominantly present in the insoluble cell debris as IBs (Fig. 2 and Fig. S1 in the supplemental material). Attempts to optimize the expression by varying the concentration of inducing agent, a change to auto-induction medium, or lower expression temperatures did not afford higher yields of soluble target protein according to sodium dodecyl sulfate (SDS)-PAGE analysis (Table S1). Nevertheless, small fractions of the TreT proteins were soluble, and enzyme activities were measured with

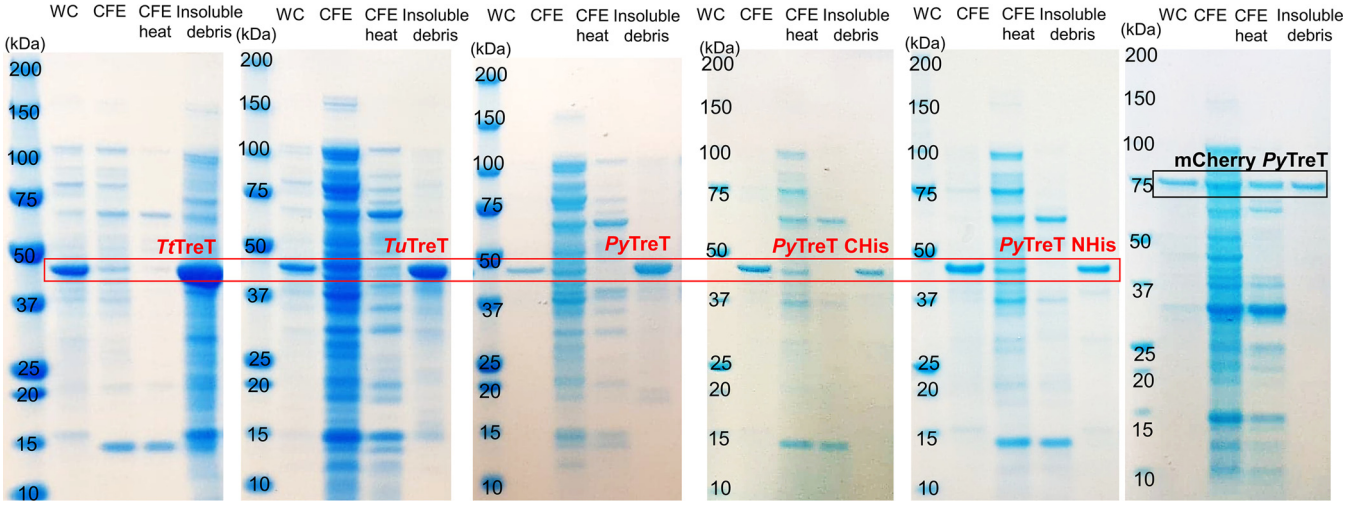

FIG 2 Comparison of whole-cell expression and protein content in the soluble and insoluble fractions analyzed by SDS-PAGE. No soluble *Tt*TreT, *Tu*TreT, *Py*TreT, or *Py*TreT with a C- or N-terminal His tag was observed in the cell extract before or after heat treatment (red box), while mCherry-*Py*TreT was highly soluble (black box). WC, whole cells; CFE, cell-free extract; CFE heat, after heat treatment of cell extract; insoluble debris, insoluble pellet after cell lysis.

high-performance liquid chromatography (HPLC) by monitoring the production of trehalose from glucose and UDP-glucose. Cell-free extracts (CFEs) of *Tt*TreT showed higher activity than those of *Tu*TreT and *Py*TreT (Table 1). Background glycosyltransferase activity from the expression host was ruled out with control experiments containing the empty plasmid.

In order to purify TreT from the soluble fraction, His_6 tags were introduced at the C or N terminus of *Py*TreT. The variant with an N-terminal His_6 tag did not bind to the nickel-Sepharose resin; the C-terminally tagged variant could be purified and showed TreT activity (Table 1). However, rapid precipitation after affinity purification resulted in fibrillar protein aggregates which could not be prevented by buffer exchange to HEPES (50 mM, pH 7.0), with the addition of 300 mM NaCl or sodium phosphate (50 mM, pH 7.0) (Fig. S2). Direct measurement of TreT activity upon purification at high temperatures showed a specific activity of 20.8 U mg^{-1}, but the continuous precipitation of protein under the given experimental conditions needs to considered.

Hyperthermostable proteins are known to show folding energy landscapes which are different from those of their mesophilic counterparts, leading more rapidly toward the formation of oligomers and aggregates during heterologous expression in a mesophilic host (41). Naturally, trehalose transferase is expressed in response to intra- or extracellular osmotic, thermal, and oxidative stresses, which coincide with the

TABLE 1 Specific activity of TreT in 400 ml of cell culture during purification

Protein or construct[b]	TreT activity by sample type or treatment (U/mg)[a]			
	CFE	Heat treatment	IB	IMAC
*Tt*TreT	0.754	0.591	0.115	NA
*Tu*TreT	0.463	0.681	0.172	NA
*Py*TreT	ND	ND	0.029	NA
*Py*TreT-CHis	ND	ND	0.050	Trace[c]
*Py*TreT-NHis	ND	ND	0.088	NA
mCherry-*Py*TreT	0.214	0.543	0.179	5.06
pBAD/His A	ND	ND	ND	ND

[a]All experiments were performed in duplicates. IMAC, immobilized metal affinity chromatography; ND, not detected; NA, not applicable.

[b]CHis, C-terminal His tag; NHis, N-terminal His tag.

[c]Separately, *Py*TreT-CHis was grown at a large scale (6× 1 liter of TB medium) and purified, and an activity of 20.8 U mg^{-1} was measured. The purified enzyme was completely precipitated 1 h after the purification. Reaction conditions were as follows: D-glucose (20 mM), UDP-D-glucose (40 mM), $MgCl_2$ (20 mM), and HEPES (50 mM, pH 7.0) at 80°C.

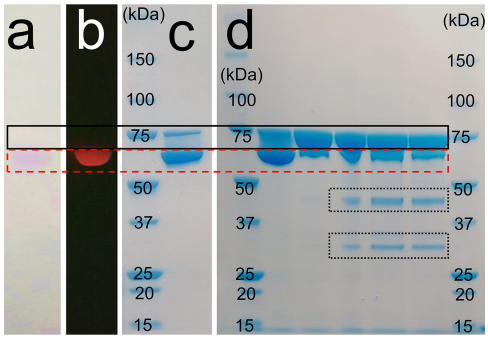

FIG 3 SDS-PAGE of SEC-purified mCherry-*Py*TreT without heat treatment showing the native fusion protein (a) and fluorescence under illumination (b, red dashed box). Subsequent staining demonstrated the appearance of the denatured protein at the expected molecular weight of mCherry-*Py*TreT (c, black box). The native mCherry-PyTreT migrated farther than the denatured protein. (d) Degradation of denatured mCherry-*Py*TreT over time at 90°C resulted in protein sizes of 29 kDa and 44 kDa (dotted black boxes), indicating hydrolysis of the amino acid linker GGSGGGGSGG.

expression of a large number of heat shock proteins and chaperones that assist in the correct folding of the native TreT protein structure within *Thermoproteus* and *Pyrobaculum* (42–48). *E. coli*, however, does not contain the same set of chaperones which would naturally occur in *Crenarchaeota* (49) and lead to misfolded protein (42–48). Furthermore, a high intracellular concentration of 0.37 mg of trehalose per mg of protein was reported for *Pyrobaculum aerophilum* (1), which potentially could stabilize TreT proteins in their native hosts and could explain the low protein stability observed *in vitro*.

Purified mCherry-*Py*TreT shows high protein solubility and stability. Due to the poor solubility of *Py*TreT, a fusion construct of mCherry and *Py*TreT containing a C-terminal His_6 tag was produced. The fusion with mCherry enables the direct quantitative spectrophotometric determination of *Py*TreT in solution, allowing rapid solubility and expression assays. *Py*TreT has a pI similar to that of mCherry and was therefore chosen as a candidate for further investigations as the fusion construct mCherry-*Py*TreT. To our satisfaction, expression of the fusion protein resulted in increased solubility for mCherry-*Py*TreT.

Typically, ≤10 mg of purified mCherry-*Py*TreT was isolated per liter of TB medium, and the formation of catalytically active IBs could not be avoided during expression (Fig. S3). The protein was purified via affinity chromatography without any concomitant precipitation occurring during purification, concentration, or repeated freezing and thawing steps at protein concentrations of up to 15 mg ml^{-1}, demonstrating increased solubility and stability of the fusion construct (Fig. 2 and Fig. S2).

The oligomerization state of mCherry-*Py*TreT was analyzed by size exclusion chromatography (SEC), and the theoretical molecular weight of 74 kDa for the fused protein was in agreement with that of a monomer of 73 kDa (Fig. S4). However, dimerization and oligomerization were also observed for mCherry-*Py*TreT at elevated protein concentrations. Although there is not much known about the increase in protein stability due to the fusion of fluorescent proteins limiting the degree of aggregation in solution, there is another example where protein stability has been increased by fusion to yellow fluorescent protein (YFP). Here, a higher oligomerization state was hypothesized to increase protein stability (50). In our case, *Py*TreT is mostly a monomer and only a dimer at high protein concentrations.

Purified mCherry-*Py*TreT was further analyzed by SDS-PAGE upon size exclusion chromatography and showed a single fluorescent purple band when the sample was not thermally denatured (Fig. 3). Upon thermal denaturation (SDS-PAGE sample buffer, 100°C), two bands were observed corresponding to residual native enzyme and denatured protein, respectively. Variation of the incubation time for thermal denaturation in SDS sample buffer did not lead to complete thermal unfolding of the protein but showed increasing hydrolysis of the fusion protein (73 kDa) into its components

mCherry (29 kDa) and *Py*TreT (44 kDa), indicating that the amino acid linker GGSGGG GSGG was hydrolyzed. In comparison, *Py*TreT showed only a single band corresponding to the unfolded protein. The fusion protein therefore showed increased stability against denaturing agents, like sodium dodecyl sulfate, suggesting an increased protein stability for mCherry-*Py*TreT. Indeed, the purified soluble mCherry-*Py*TreT proved to be stable in 2% SDS in Tris buffer (50 mM, pH 8.0) when the absorption spectra were measured spectrophotometrically, showing no protein denaturation.

Direct spectrophotometric protein quantification of an mCherry-*Py*TreT fusion protein. The fusion of the thermostable protein mCherry to *Py*TreT not only improved protein stability but also provided a rapid spectroscopic method for protein quantitation. The molar extinction coefficient of the fusion protein mCherry-*Py*TreT was calculated from the protein concentration as determined by a bicinchoninic acid (BCA) assay and the UV/visible light (UV/Vis) spectrum of the native protein, which showed an absorbance maximum at 578 nm (Fig. S5). Using the alkali denaturation method, the mCherry chromophore could be converted into the well-studied green fluorescent protein chromophore with a known molar extinction coefficient (ε) of 44,000 M^{-1} cm^{-1} and a corresponding shift in the absorbance maximum from 587 nm to 455 nm. Based on these two values, a molar extinction coefficient of $\varepsilon_{mcherry\text{-}PyTreT} = 73476\ M^{-1}\ cm^{-1}$ could be derived for the mCherry fusion protein, which matched the reported value in the literature of 72,000 M^{-1} cm^{-1} for mCherry (51). Using the calculated molar extinction coefficient of 73,476 M^{-1} cm^{-1}, a protein concentration of 2.34 μM was determined spectrophotometrically, in good agreement with a protein concentration of 2.50 μM in the BCA assay for mCherry-*Py*TreT.

Nonclassical IBs of TreT show glycosyltransferase activity. The formation of insoluble aggregates during recombinant expression is driven by the association of correctly, partially, and misfolded proteins (52). Classical inclusion bodies are described as aggregates of misfolded proteins with complete loss of function (53). However, "nonclassical" IBs are described as aggregates that contain fully or partially functional proteins which can be purified by the removal of contaminating membrane-bound proteins by mild solubilization agents like deoxycholic acid (DOC) (54).

The removal of other proteins with 1% (wt/wt) DOC resulted in excellent purity of TreT in all cases (Fig. S1). The TreT content within inclusion bodies proved to be between 1% and 5% protein in wet inclusion bodies (Fig. S6). In the case of the fluorescent mCherry-*Py*TreT, spectrophotometric analysis showed that 68% (wt/wt) mCherry-*Py*TreT was correctly folded.

IBs from all TreT variants showed high glycosyltransferase activity between 0.02 and 0.18 U mg^{-1}, as is shown in Fig. 4. Diffusion limitations within inclusion bodies could lower the observed reaction rate in comparison to that of the soluble protein, which could be optimized via the increase of temperature or formulation of inclusion bodies. Comparable amounts of IBs were utilized for the conversion of benzaldehyde to (*R*)-mandelonitrile with catalytically active inclusion bodies of hydroxynitrile lyases (55). The feasibility of IBs as immobilized biocatalysts has increased the interest in using them for synthetic purposes (56, 57). However, this study aimed at the biochemical characterization of soluble TreT, and the application, further optimization, and formulation of TreT IBs were therefore not further pursued beyond the proof of concept.

Kinetic characterization and thermal stability of mCherry-*Py*TreT. The glycosyltransferase activity of mCherry-*Py*TreT was determined by HPLC analysis (Fig. S7 and Table S2). A temperature optimum for protein stability was determined to be 60°C (Fig. 5), and a V_{max} of 11.39 $\pm$ 0.29 U mg^{-1} and K_m of 0.61 $\pm$ 0.11 mM were obtained for UDP-glucose. The kinetic constants at temperatures above 60°C were not investigated due to the degradation of UDP-glucose under these conditions. In comparison, other investigators have shown a V_{max} of 184 U mg^{-1} and K_m (UDP-glucose) of 0.23 mM for *Tt*TreT using a coupled assay at 80°C (21). For D-glucose, noncompetitive substrate inhibition was observed, with a K_m (glucose) of 2.30 $\pm$ 0.58 mM, a K_i (glucose) of

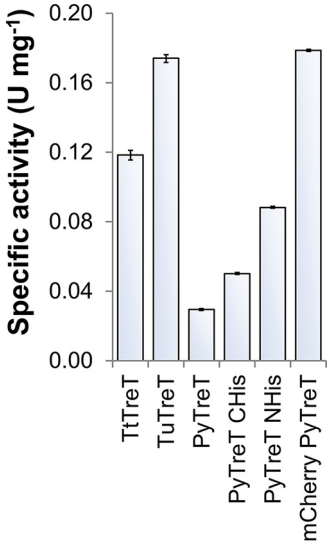

FIG 4 Specific activity of purified TreT IBs. Reaction conditions were as follows: 50 mM HEPES (pH 7.0), 20 mM $MgCl_2$, 40 mM UDP-glucose, 10 mM glucose, and 3.0 to 5.0 mg of TreT IB at 60°C. CHis, C-terminal His tag; NHis, N-terminal His tag.

10.63 ± 2.21 mM, and a V_{max} of 17.06 ± 2.22 U mg^{-1}. Substrate inhibition has not been reported for other TreT proteins (21).

mCherry-*Py*TreT was incubated for 2 h at 60, 70, 80, and 90°C, and residual enzyme activities are shown in Fig. 5a and Fig. S8. Residual protein activities were found to correlate with the residual absorbance from mCherry. The initial rate of the enzyme increased exponentially with temperature according to the Arrhenius equation, showing the highest activity at 80°C (Fig. 5b), and a Gibbs free energy of activation, $\Delta G^{\ddagger}$, of 92.7 kJ mol^{-1} was determined from the Arrhenius plot (Fig. 5c).

The effect of pH, cations, and anions on the activity of mCherry-*Py*TreT. The fusion protein mCherry-*Py*TreT showed a broad pH stability over a pH range of 5 to 9 (Fig. 6a). The optimal pH was found at pH 6.0, which is similar to the pH optimum of a trehalose transferase from *Thermococcus litoralis* (25). Divalent cations could potentially form chelates with the phosphate group of the sugar donor substrate and thereby influence the substrate binding and enzyme activity. A wide range of metal salts were explored to account for potential chaotropic and kosmotropic effects of the counter anions. As can be seen in Fig. 6b, the addition of sodium chloride slightly inhibited the enzyme, while sodium sulfate did not. The enzyme activity was found to increase with

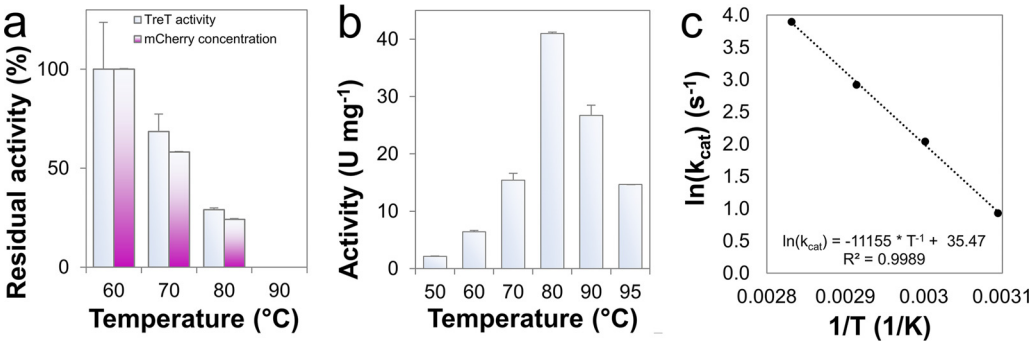

FIG 5 (a) The thermostability of mCherry-*Py*TreT after 2 h of incubation at 60, 70, 80, and 90°C is shown (1.0 mg ml^{-1} mCherry *Py*TreT, 50 mM HEPES, pH = 7.0). (b) The initial activity of mCherry-*Py*TreT depending on temperature, showing deactivation after 80°C. (c) Arrhenius plot of the initial enzyme activity from 50 to 80°C. Reaction conditions were as follows: 50 mM HEPES (pH 7.0), 20 mM $MgCl_2$, 40 mM UDP-glucose, and 10 mM glucose, and temperatures between 50°C and 95°C. *T*, temperature (in kelvins).

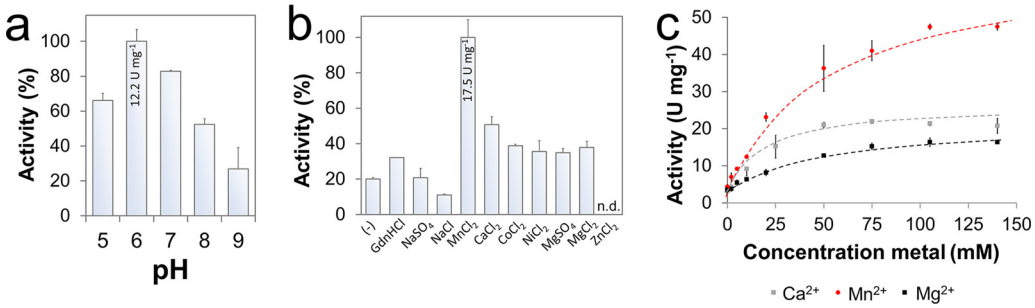

FIG 6 (a) The enzyme activity of mCherry-*Py*TreT using a multicomponent buffer shows a broad pH distribution. (b) Effect of different cations and anions (20 mM) on enzyme activity. (c) Enzyme saturation kinetics of the three best metals were investigated. Reaction conditions were as follows: 50 mM HEPES (pH 7.0) or the multicomponent buffer, 20 mM $MgCl_2$ or 20 mM additive, 40 mM UDP-glucose, and 10 mM glucose at 60°C.

the addition of metal chloride salts in the following order: $Mg^{2+} \sim Ni^{2+} < Co^{2+} < Ca^{2+} < Mn^{2+}$; addition of Zn^{2+} resulted in the complete inhibition of the enzyme. A similar behavior was reported for a trehalose transferase from *T. litoralis*, where zinc(II) chloride completely inhibited the enzyme (25). No difference in enzyme activity was observed when magnesium chloride was replaced with magnesium sulfate. Surprisingly, the strong chaotrope guanidine hydrochloride increased the enzyme activity similarly to magnesium(II). Apparent dissociation constants ($K_{d,app}$s) of 44 ± 8 mM, 21 ± 5 mM, and 18 ± 5 mM were determined for Mn(II), Ca(II), and Mg(II), respectively, by measuring the enzymatic trehalose production, as is shown in Fig. 6c and Table S2. The apparent maximal rate at saturating concentrations ($V_{sat,app}$) followed the inverse trend, with Mn(II) > Ca(II) > Mg(II) (59 ± 3 U mg^{-1}, 24 ± 1 U mg^{-1}, and 18 ± 1 U mg^{-1}, respectively). A similar dependency of the enzyme reaction rate on the presence of divalent cations has also been reported for a UDP-dependent glycogen synthase (58) and for α-fucosyltransferase V (59). However, no difference in activation has been described for the trehalose transferase from *Thermococcus litoralis* for manganese(II) or magnesium(II) (25).

To delineate the different effects of Mg(II), Ca(II), Mn(II) on the K_d and V_{sat}, the protein stability of the mCherry-*Py*TreT metal complex was investigated. The observed protein melting temperatures (T_ms) for Mn(II), Ca(II), and Mg(II) were 75°C, 82°C, and 82°C, respectively, indicating that chaotropic divalent cations reduce the enzyme's conformational stability (Fig. S9). Moreover, the melting pattern showed faster denaturation of mCherry-*Py*TreT for Ca(II) than for Mg(II) despite similar T_ms. This indicates that calcium destabilizes the protein to a higher degree.

Reaction equilibrium of trehalose transferase-catalyzed reactions is dependent on the nature of the nucleotides and nucleotide carbohydrates. Like any other catalyst, enzymes enhance the rate of reaction toward thermodynamic equilibrium. However, it has been suggested that *Tt*TreT only catalyzes the forward reaction in the synthesis direction when UDP and UDP-glucose are used (21), while the trehalose transferase from *Pyrococcus horikoshii* has been shown to catalyze the reaction reversibly using a wide range of nucleotide diphosphates (Fig. 7) (24).

While the thermodynamic equilibrium for the enzyme-catalyzed synthesis of trehalose from glucose and a nucleotide sugar lies in favor of the product trehalose for both

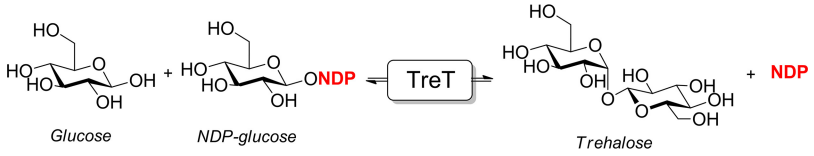

FIG 7 The overall reaction of α,α-(1→1) coupling of α-D-glucose and NDP-D-glucose to synthesize trehalose and nucleotide diphosphate (NDP), which is either ADP or UDP.

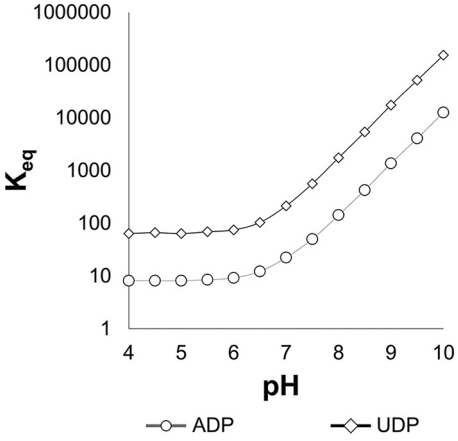

FIG 8 The influence of pH on the thermodynamic equilibrium of the coupling of glucose and UDP- or ADP-glucose to trehalose and UDP or ADP was calculated by eQuilibrator, version 2.0 (http://equilibrator.weizmann.ac.il/).

UDP and ADP as nucleotides, the magnitude of the K_{eq} depends on the respective nucleotide sugar used. The synthesis of trehalose using an excess of UDP- or ADP-glucose and glucose with mCherry-*Py*TreT leads to quantitative conversion of glucose, while the reverse reaction of trehalose with UDP or ADP leads to the formation of glucose and UDP- or ADP-glucose. According to HPLC analysis, a low specific activity for ADP (98 mU mg^{-1}) versus that of UDP (290 mU mg^{-1}) was observed, and K_{eq} values of 157 for UDP and 30 for ADP were determined experimentally (Fig. S10). Analysis of previously reported data showed that reactions with TreT from *Pyrococcus horikoshii* were found to establish equilibrium concentrations with K_{eq} values of ~230 for UDP and ~29 for ADP (24). Hence, it was shown for different TreT enzymes that they catalyze both the forward and reverse reactions and that the final conversions depend on the utilized nucleotide sugar, where product formation is favored by use of UDP over that of ADP.

Overall, the thermodynamic equilibrium K_{eq} for the synthesis of trehalose and UDP from glucose and UDP-glucose also depends on the pH, metal ion composition, and ionic strength. Although chelation of divalent cations with the phosphate moiety of the nucleotide is not included in the estimation of Gibbs free energies of formation, the equilibrium constants (K_{eq}s) for the formation of trehalose from glucose using uridine or ADP glucose at various pH values could be estimated with the thermodynamic calculator eQuilibrator, version 2.0 (see the supplemental material) (60). Equilibrium constants of 23 and 225 were calculated for ADP and UDP, respectively, which reasonably matched the values that were observed experimentally (K_{eq} values of 30 and 157, respectively). Based on this, our calculations predict a shift of the equilibrium constant toward the starting materials under increasingly acidic conditions due to the protonation of UDP (pKa 5.5 to 6.5 [61, 62]) (Fig. 8 and Tables S3 to S6). A similar pH dependence has been reported for UDP-dependent sucrose synthase (62). The application of eQuilibrator, version 2.0, to determine thermodynamic equilibria has successfully been implemented with sucrose synthase by other investigators (62).

DISCUSSION

None of the trehalose transferases investigated here, each having a different isoelectric point, showed an increased solubility resulting in the formation of inclusion bodies *in vivo* and aggregation of soluble protein *in vitro*. While our results clearly showed an increase in protein solubility and stability through the fusion of *Py*TreT with mCherry, the exact mechanism behind these observations remains elusive. mCherry might function as a molecular chaperone by stabilizing aggregation-prone folding intermediates, which previously has also been suggested for the maltose binding protein (63). Furthermore, self-oligomerization of correctly folded TreT might be re-

duced due to the increased size of the fusion protein. While other solubility tags potentially could have achieved similar results (64), the use of mCherry as a thermostable, fluorescent protein tag allowed rapid spectrophotometric protein quantification and exhibited excellent reaction compatibility with a thermostable enzyme.

The biochemical characterization of mCherry-*Py*TreT showed noncompetitive substrate inhibition for glucose, which was not reported earlier for other trehalose transferases. A structural explanation for noncompetitive inhibition would be the binding of a sugar acceptor in the binding site for the nucleotide sugar donor. A comparison with untagged *Py*TreT was not possible due to its aggregational behavior, and therefore we cannot exclude an effect of the mCherry fusion on the kinetic properties of TreT. Due to the length of the linker and the distance of mCherry to the active site of *Py*TreT, it is not likely that the kinetic parameters would be drastically different. The observed rate of enhancement in the presence of chloride salts of guanidine, Mg(II), Ca(II), and Mn(II) could be explained by either a decrease of enzyme rigidity by chaotropic agents or complexation of the metal with the diphosphate-group of UDP and/or UDP-glucose or by a combination of the two. Considering the observation, that guanidinium hydrochloride similarly increased the enzyme activity, this study suggests that enzyme rigidity is a controlling factor in mCherry-*Py*TreT and that chaotropic agents can increase the enzyme flexibility and thereby the activity. This is not surprising since meso- and thermophilic proteins have earlier been shown to demonstrate catalytic enhancement by the addition of chaotropic agents, leading to a decrease in the intrinsically high conformational rigidities of thermostable proteins (65). Indeed, a conformational change of ca. 4 Å has been observed between the sugar donor and acceptor binding domains for the protein crystal structure of TreT from *Pyrococcus horikoshii* (PDB accession number 2X6Q), which closes upon substrate binding (PDB accession number 2XMP), highlighting the importance of conformational flexibility (23). Moreover, conformational flexibility upon substrate binding has also been observed for trehalose phosphate synthase (OtsA) from *E. coli* K-12 (66), glycogen synthase (58), and α-fucosyltransferase V (59). Assuming that enzyme mobility is rate limiting, chaotropic reagents plausibly explain increased TreT activity. On the other hand, Zn(II) completely inhibited the activity of mCherry-*Py*TreT and TreT from *Thermococcus litoralis* (25), emphasizing the effect that complexation of metals with the diphosphate moiety of the nucleotide sugar donor can have.

Conclusion. To conclude, the fusion of mCherry to *Py*TreT showed that an intrinsically aggregation-prone protein could be stabilized in solution and offered a tool to monitor protein solubility by UV-Vis spectroscopy. This allowed the biochemical characterization of mCherry-*Py*TreT at elevated temperatures, which showed increased activity using manganese(II) and the chaotropic reagent guanidine hydrochloride. Furthermore, our results highlight that the equilibrium constant for the synthesis or hydrolysis of trehalose is determined by the composition of the reaction mixture, where the utilization of different nucleotides and pH values can substantially shift the equilibrium. Trehalose transferases are therefore not unidirectional, and the use of a specific nucleotide or nucleotide sugar determines the overall conversion. The production and biochemical characterization of the stable mCherry-*Py*TreT fusion protein addressed one of the major problems of archaeal glycosyltransferases and is therefore of particular relevance for the industrial production of novel disaccharides and nucleotide carbohydrates, providing insight into the optimal process conditions and thermodynamic limitations in using trehalose transferases.

MATERIALS AND METHODS

Chemicals. The following chemicals were used: uridine 5′-diphosphate disodium salt (98%; Carbosynth), D-glucose (99.5%; Sigma-Aldrich), HEPES (>99.5%; Sigma-Aldrich), $MgCl_2$ hexahydrate (>99.5%; VWR), $CaCl_2$ dihydrate (>99.0%; Sigma-Aldrich), $NiCl_2$ hexahydrate (99.9%), guanidine hydrochloride (>99.5%; Sigma-Aldrich), sodium deoxycholate (>98%; Sigma-Aldrich), sodium sulfate (>99.0%; Sigma-Aldrich), zinc chloride (>98%; Sigma-Aldrich), magnesium sulfate heptahydrate (99%; Sigma-Aldrich), cobalt chloride hexahydrate (>98%; Sigma-Aldrich), glycerol (99.5%; Sigma-Aldrich), rubidium chloride (>99%; Sigma-Aldrich), potassium acetate (>99%; Acros), sulfuric acid (98%; Acros), agarose (>99%;

Sigma-Aldrich), ampicillin (Sigma-Aldrich), Tris(hydroxymethyl)aminomethane (Tris, 99%; Sigma-Aldrich), glycine (>99%; Sigma-Aldrich), pyridine (>99%; Sigma-Aldrich), sodium chloride (>99.5%; J.T. Baker), bis-Tris (>99%; Sigma-Aldrich), acetonitrile (ACN) (>99.5%; Sigma-Aldrich), UDP disodium salt (>96%; Sigma-Aldrich), ADP disodium salt (bacterial, >95%; Sigma-Aldrich), and adenosine 5′-diphosphoglucose disodium salt (>93%; Sigma-Aldrich).

Materials. A QIAprep Miniprep kit was purchased from Qiagen. The high-fidelity (HF) restriction endonucleases KpnI HF, SacI HF, BamHI HF, and NcoI HF were used with a standard protocol using 10× CutSmart buffer (New England Biolabs). Purification of plasmids from agarose gel was performed with a Monarch DNA gel extraction kit (New England Biolabs) using a standard protocol. Ligation was performed using a standard protocol with T7 DNA ligase and T7 DNA ligase reaction buffer (New England Biolabs).

Analytical instruments. Chromatographic analysis of reaction products was performed using a Shimadzu high-performance liquid chromatography (HPLC) system equipped with an Imtakt Unison-UK amino column (0.4 by 25 cm, 60°C), an evaporative light-scattering detector (ELSD) (Shimadzu ELSD-LTII), a UV detector (SPD-20A), and acetonitrile-water-formic acid at 80:20:0.1 as the mobile phase (1 ml min^{-1}). The samples were calibrated using an external calibration curve, as is shown in Fig. S11 in the supplemental material.

BCA assay. Protein content was determined with a BCA protein quantitation kit (Thermo Scientific, Carlsbad, CA, USA). Standard curves were prepared with bovine serum albumin (BSA) in the range of 0.01 to 2 mg ml^{-1} in (poly)styrene 96-well plates. Samples were measured in triplicate and monitored at 562 nm utilizing a microtiter plate spectrophotometer (Synergy 2; BioTek). A protocol for the solubilization of inclusion bodies in 2% SDS in Tris-HCl buffer (50 mM, pH 8.0) was adopted from the literature (54). The negative control containing 2% SDS in Tris-HCl buffer (50 mM, pH 8.0) does not show a background absorption with the BCA reagent buffer.

SDS-PAGE. Protein samples were denatured using XT sample buffer (Bio-Rad) supplied with XT reducing agent (Bio-Rad) at 95°C for 15 min. Gel electrophoresis was performed with Criterion XT 4 to 12% bis-Tris precast gels (Bio-Rad) using morpholinepropanesulfonic acid (MOPS) buffer (Bio-Rad). The gels were run at 150 V for 40 to 60 min and stained with SimplyBlue SafeStain (Novex). A Precision Plus Protein Unstained Standard (Bio-Rad) was used to determine the relative molecular mass of the protein.

Spectrophotometric measurements. The absorbance of mCherry-*Py*TreT at wavelengths of 190 to 800 nm ($\lambda_{190-800}$) was measured utilizing a 1-cm quartz cuvette. All measurements for the determination of the molar extinction coefficient were performed in triplicates.

Growth media. Terrific broth medium consisting of 1.20% (wt/wt) tryptone, 2.40% (wt/wt) yeast extract, 53 mM K_2HPO_4, 16 mM KH_2PO_4, and 4% (wt/wt) glycerol was autoclaved at 121°C for 20 min. Auto-induction medium ZYM-5052 was prepared according to literature protocols (67). LB medium consisting of 1.00% (wt/wt) tryptone, 0.5% (wt/wt) yeast extract, and 1% NaCl was autoclaved at 121°C for 20 min. All media were supplemented with 100 μg ml^{-1} ampicillin.

Bacterial plasmids and strains. The plasmid pBAD/His A (Invitrogen) was provided by the commercial suppliers. The strains *E. coli* DH5α, with the genotype λ^- ϕ80d*lacZ*ΔM15 Δ(*lacZYA-argF*)*U169 recA1 endA1 hsdR17*(r_K^- m_K^-) *supE44 thi-1 gyrA relA1*, and *E. coli* Top10, with the genotype F^- *mcrA* Δ(*mrr-hsdRMS-mcrBC*) φ80*lacZ*ΔM15 Δ*lacX74 recA1 araD139* Δ(*ara-leu*)*7697 galU galK rpsL* (Str^r) *endA1 nupG*, were ordered from New England Biolabs and Invitrogen, respectively.

Preparation of competent cells with rubidium chloride. Competent cells of *E. coli* DH5α and *E. coli* Top10 were prepared with rubidium chloride. Cells from an overnight culture were grown to an optical density at 600 nm (OD_{600}) of 0.5 in LB medium and centrifuged (425 relative centrifugal force [rcf], 15 min, 4°C). The LB medium was decanted, and the cells were washed in 30 ml of freshly prepared ice-cold solution rubidium chloride (100 mM), manganese(II) chloride (10 mM), potassium acetate (3 mM), calcium chloride (1 mM), and glycerol (165 mM), followed by centrifugation at 2,000 rpm (5 min, 4°C). The cells were resuspended in 4 ml of MOPS buffer (100 mM, pH 7.0) containing RbCl (10 mM), $CaCl_2$ (5 mM), and glycerol (165 mM), and 0.1 ml was aliquoted in ice-cold polypropylene Eppendorf tubes. The competent cells were stored at −80°C.

Transformation. The synthesized, lyophilized DNA (Baseclear, Leiden) was briefly centrifuged (425 rcf, 30 s), and resuspended in 40 μl of Tris buffer (10 mM, pH 8.5) and diluted 1:10. The DNA concentrations measured via the absorbance at 260 nm showed DNA concentrations of 200 ng μl^{-1} and 20 ng μl^{-1} for the undiluted (1:1) and diluted (1:10) samples, respectively. The competent cells were thawed, and the pUC-SP plasmids containing the synthesized gene were added to reach final concentrations of ~8 ng μl^{-1} and ~1.6 ng μl^{-1}, respectively. After 30 min of incubation on ice, the competent cells were heat treated at 42°C for 30 s. To the solution, 500 μl of sterile LB medium was added and incubated for 1 h at 37°C, followed by plating on agar plates containing the ampicillin (100 μg ml^{-1}).

Cloning and expression of TreT from in *E. coli* Top10. The pUC-SP vector containing the codon-optimized and synthetic TreT genes was transformed in chemically competent *E. coli* DH5α strains and stored as glycerol stocks at −80°C. The *E. coli* strain was grown in LB medium containing 100 μg ml^{-1} ampicillin overnight at 37°C, and the plasmid was isolated (QIAprep Miniprep; Qiagen).

The *treT*-containing pUC-SP and pBAD/His A plasmids were digested with KpnI and NcoI. The digested fragments were purified on a 1% agarose gel after gel electrophoresis (120 V; Bio-Rad) using the standard protocol of the Monarch DNA gel extraction kit (New England BioLabs). After ligation with T7 ligase at 16°C overnight using the provided protocol (New England BioLabs), the plasmid was transformed into competent *E. coli* Top10 cells and sequenced (BaseClear, Leiden).

Production and purification of recombinant TreT from in *E. coli* Top10 pBAD/His A. (i) Preparation of cell extract. The 5-ml inoculum of *E. coli* Top10(pBAD/His A) containing *Tt*TreT, *Tu*TreT, *Py*TreT,

N- or C-terminally His-tagged *Py*TreT, and mCherry *Py*TreT genes was grown in LB medium containing 100 μg ml^{-1} ampicillin at 37°C overnight. To seven 2-liter baffled Erlenmeyer flasks containing 400 ml of TB-medium, 5 ml of inoculum was added (1.3%, vol/vol) and induced with L-arabinose to a final concentration of 0.02% (wt/wt) after the culture reached an OD_{600} of 0.6 to 0.8. The cells were harvested at the OD_{600} after 14 h by centrifugation (17,000 $\times$ *g*, 15 min, 4°C), followed by resuspension of the wet cell pellet in 25 ml of lysis buffer containing Tris-HCl buffer (50 mM, pH 7.4), imidazole (20 mM), lysozyme (0.5 mg ml^{-1}), and DNase I (0.1 mg ml^{-1}) per gram of wet cells. After 30 min of incubation on ice, the cells were passed through a cell disruptor (1.35 $\times$ 10^8 Pa) for three consecutive rounds. The cell debris was collected via centrifugation at 12,000 rpm (Fiberlite F12-6 $\times$ 500 LEX, 10 min, 20°C [Sorvall]), and the CFE was obtained via decantation.

(ii) Immobilized nickel affinity chromatography. The CFE was heat treated at 60°C for 20 min in a water bath. The precipitates in the CFE were removed via centrifugation at 12,000 rpm (Fiberlite F12-6 $\times$ 500 LEX, 10 min, 20°C [Sorvall]), and the heat-treated CFE was obtained via decanting. The heat-treated CFE was purified using affinity chromatography on a 1-ml nickel-Sepharose column by charging CFE on the column for at least three consecutive rounds using a peristaltic pump (Bio-Rad). The column was washed with binding buffer (20 mM Tris-HCl, 500 mM NaCl, 20 mM imidazole, pH 7.4) until no protein eluted. The bound enzyme was eluted using elution buffer (20 mM Tris-HCl, 500 mM NaCl, 500 mM imidazole, pH 7.4). Protein samples were concentrated in a 12-ml Amicon Ultra centrifugal filter (30 kDa; Merck). Elution buffer was exchanged for HEPES (50 mM, pH 7.0) containing $MgCl_2$ (20 mM) by three consecutive rounds of washing with 12-ml Amicon Ultra centrifugal filters (30 kDa; Merck) and analyzed by SDS-PAGE and HPLC.

(iii) Purification of inclusion bodies. A literature protocol was adopted (68). The insoluble debris was homogenized in 20 ml of Tris-HCl buffer (50 mM, pH 8.5) containing 1% (wt/wt) deoxycholic acid. The solubilized trehalose transferases were separated from the inclusion bodies via centrifugation (20,000 $\times$ *g*, 15 min, 20°C) and is referred to as the washing solution. The solubilization and centrifugation were repeated two times, resulting in solubilized washing solutions 1, 2, and 3. Next, Tris-HCl buffer (50 mM, pH 8.5) was utilized to remove the remaining DOC. The inclusion bodies were harvested via centrifugation (20,000 $\times$ *g*, 15 min, 20°C), and the solutions were analyzed by SDS-PAGE for protein purity.

Production and purification of soluble recombinant C-terminally His-tagged TreT from *Pyrobaculum yellowstonensis* WP30 in *E. coli* Top10(pBAD/His A). The protocol described above was repeated six times with 5-liter Erlenmeyer flasks containing 1 liter of TB medium. The isolated cell extract was purified using a prepacked 5-ml HisTrap FF column (GE Healthcare) and analyzed by SDS-PAGE and HPLC. Reaction conditions were the following: D-glucose (10 mM), UDP-glucose (0 to 50 mM), HEPES (50 mM, pH 7.0), *Py*TreT (0.02 mg ml^{-1}), and 20 mM magnesium(II) chloride at 80°C.

Production and purification of soluble recombinant mCherry-*Py*TreT in *E. coli* Top10(pBAD/His A). The cell extract was prepared as described above, containing 1 liter of TB medium in an Erlenmeyer flask. All of the other steps were sized accordingly, using a 12-ml prepacked HisTap FF column for purification. As an additional purification step, the protein was purified using a Superdex 200 Increase 10/300 GL column with HEPES (50 mM, pH 7.4) buffer containing 300 mM NaCl as a mobile phase. The column was calibrated with a gel filtration standard (catalog number 151-1901; Bio-Rad) containing a lyophilized mix of thyroglobulin (M_w, 670 kDa), bovine gamma globulin (M_w, 158 kDa), chicken ovalbumin (M_w, 44 kDa), equine myoglobin (M_w, 17 kDa), and vitamin B_{12} (M_w, 1.35 kDa) before use. The eluate was concentrated using a 12-ml Amicon Ultra centrifugal filter (30 kDa; Merck) yielding 1 mg per liter of LB medium. The sample was analyzed by SDS-PAGE and HPLC.

Quantification of D-glucose and D-trehalose with HPLC. Samples during activity assays were quenched by the addition of 50 μl of reaction solution to an equal volume of ice-cold HPLC-grade acetonitrile and incubated at −80°C for 1 h. The samples were centrifuged at 14,000 rpm for 10 min at 4°C. The supernatant was collected and analyzed by HPLC (Imtakt UK-Amino 250- by 4.6-mm column, 50°C, ELSD, 80:20 ACN-H_2O, 1.0 ml min^{-1}). Enzyme activity was calculated with external standards for trehalose using the slope of at least three different substrate concentrations. The enzyme activity was determined in duplicates.

For D-glucose, the reaction conditions were varied, and the mixture contained D-glucose (0 to 35 mM), UDP-glucose (40 mM), HEPES (50 mM, pH 7.0), mCherry-*Py*TreT (0.02 mg ml^{-1}), and $MgCl_2$ (20 mM). The reaction mixture was incubated at 60°C with gentle shaking. The data were fitted (Gnuplot, version 5.2) to the equation shown in Table S2.

For the kinetic analysis of UDP-glucose, the reaction conditions were varied, and the mixture contained D-glucose (10 mM), UDP-glucose (0 to 50 mM), HEPES (50 mM, pH 7.0), mCherry-*Py*TreT (0.02 mg ml^{-1}), and 20 mM magnesium(II) chloride. The reaction mixture was incubated at 60°C with gentle shaking. The data were fitted (Gnuplot, version 5.2) to the equation shown in Table S2.

For the evaluation of enzyme activity and kinetic analysis of different cations or anions, the reaction conditions were varied, and the mixture contained D-glucose (10 mM), UDP-glucose (40 mM), HEPES (50 mM, pH 7.0), mCherry-*Py*TreT (0.02 mg ml^{-1}), and either guanidine hydrochloride (20 mM), sodium sulfate (20 mM), sodium chloride (20 mM), manganese(II) chloride (0 to 140 mM), calcium(II) chloride (0 to 140 mM), cobalt(II) chloride (20 mM), nickel(II) chloride (20 mM), magnesium(II) sulfate (20 mM), magnesium(II) chloride (0 to 140 mM), or zinc(II) chloride (20 mM). The reaction mixture was incubated at 60°C with gentle shaking. The data were fitted (Gnuplot, version 5.2) to the equation shown in Table S2.

The effect of pH was evaluated using a multicomponent buffer containing D-glucose (10 mM), UDP-glucose (40 mM), mCherry-*Py*TreT (0.02 mg ml^{-1}), pyridine (15 mM), bis-Tris (15 mM), HEPES

(15 mM), glycine (15 mM), $MgCl_2$ (20 mM), and NaCl (150 mM). The reaction mixture was incubated at 60°C with gentle shaking. The enzyme activity was determined in duplicates.

The reaction temperature was varied between 50 and 95°C with gentle shaking using a mixture containing D-glucose (10 mM), UDP-glucose (40 mM), HEPES (50 mM, pH 7.0), mCherry-*Py*TreT (0.02 mg ml^{-1}), and $MgCl_2$ (20 mM). The enzyme activity was determined in duplicates.

To assess the stability of mCherry-PyTreT a 1-ml stock solution containing 1.0 mg ml^{-1} was incubated between 50 and 80°C, and the absorbance (587 nm) was measured in a 1-cm polyacrylate cuvette. The enzyme activity was measured using D-glucose (10 mM), UDP-glucose (40 mM), HEPES (50 mM, pH 7.0), mCherry-*Py*TreT (0.02 mg ml^{-1}), and $MgCl_2$ (20 mM) at 60°C. The enzyme activity was determined in duplicates using HPLC analysis.

Thermal shift assays. The melting temperature under different solution conditions containing Mn(II), Ca(II), or Mg(II) was determined by using a thermal shift assay (or differential scanning fluorimetry [DSF]). Briefly, mCherry-*Py*TreT was diluted in HEPES buffer (50 mM, pH 7.0) containing 20 mM divalent cation, 300 mM NaCl, and SYPRO Orange solution (S-6651; ThermoFisher Scientific). The microplate was sealed with an adhesive optical clear seal (MicroAmp optical adhesive film), centrifuged at 4°C for 30 s, and heated from 5 to 95°C, with increments of 1°C/min, using a reverse transcription-PCR (RT-PCR) instrument (StepOnePlus Real-Time PCR System; Applied Biosystems). Fluorescence in each well was followed by applying excitation and emission wavelengths of 485 nm and 530 nm, respectively. The melting temperature (T_m) corresponds to the temperature at which the protein is 50% unfolded.

Determination of thermodynamic equilibrium of the trehalose transferase reaction using mCherry-*Py*TreT. Reaction equilibrium was determined via the addition of enzyme. For the forward reaction, D-glucose (10 mM), UDP- or ADP-glucose (40 mM), HEPES (50 mM, pH 7.0), mCherry-*Py*TreT (1.0 mg ml^{-1}), and $MgCl_2$ (20 mM) were evaluated by monitoring the production of trehalose. For the reverse reaction, D-trehalose (10 mM), UDP or ADP (40 mM), HEPES (50 mM, pH 7.0), mCherry-*Py*TreT (1.0 mg ml^{-1}), and $MgCl_2$ (20 mM) were utilized to follow the production of D-glucose. The enzyme activity was determined in duplicates using HPLC analysis. The thermodynamic equilibrium was determined from the last three data points, as shown in Fig. S10.

SUPPLEMENTAL MATERIAL

Supplemental material for this article may be found at https://doi.org/10.1128/AEM.03084-18.

SUPPLEMENTAL FILE 1, PDF file, 0.9 MB.

ACKNOWLEDGMENT

This research was supported by grant ERA-IB-15-110 of the ERA-NET on Industrial Biotechnology.

REFERENCES

1. Martins LO, Huber R, Huber H, Stetter KO, Da Costa MS, Santos H. 1997. Organic solutes in hyperthermophilic Archaea. Appl Environ Microbiol 63:896–902.
2. Conlin LK, Nelson HCM. 2007. The natural osmolyte trehalose is a positive regulator of the heat-induced activity of yeast heat shock transcription factor. Mol Cell Biol 27:1505–1515. https://doi.org/10.1128/MCB.01158-06.
3. Fernandez O, Béthencourt L, Quero A, Sangwan RS, Clément C. 2010. Trehalose and plant stress responses: friend or foe? Trends Plant Sci 15:409–417. https://doi.org/10.1016/j.tplants.2010.04.004.
4. Liu K, Dong Y, Huang Y, Rasgon JL, Agre P. 2013. Impact of trehalose transporter knockdown on *Anopheles gambiae* stress adaptation and susceptibility to *Plasmodium falciparum* infection. Proc Natl Acad Sci U S A 110:17504–17509. https://doi.org/10.1073/pnas.1316709110.
5. Martin DD, Ciulla RA, Roberts MF. 1999. Osmoadaptation in Archaea. Appl Environ Microbiol 65:1815–1825.
6. Ajito S, Hirai M, Iwase H, Shimizu N, Igarashi N, Ohta N. 2018. Protective action of trehalose and glucose on protein hydration shell clarified by using X-ray and neutron scattering. Physica B Condens Matter 551:249–255. https://doi.org/10.1016/j.physb.2018.03.040.
7. Cordone L, Cottone G, Giuffrida S. 2007. Role of residual water hydrogen bonding in sugar/water/biomolecule systems: a possible explanation for trehalose peculiarity. J Phys Condens Matter 19:205110. https://doi.org/10.1088/0953-8984/19/20/205110.
8. Schebor C, Burin L, Buera MDP, Chirife J. 1999. Stability to hydrolysis and browning of trehalose, sucrose and raffinose in low-moisture systems in relation to their use as protectants of dry biomaterials. LWT Food Sci Technol 32:481–485. https://doi.org/10.1006/fstl.1999.0576.
9. Zhang R, Pan YT, He S, Lam M, Brayer GD, Elbein AD, Withers SG. 2011. Mechanistic analysis of trehalose synthase from *Mycobacterium smegmatis*. J Biol Chem 286:35601–35609. https://doi.org/10.1074/jbc.M111.280362.
10. Asthana RK, Srivastava S, Singh AP, Kayastha AM, Singh SP. 2005. Identification of maltooligosyltrehalose synthase and maltooligosyltrehalose trehalohydrolase enzymes catalysing trehalose biosynthesis in *Anabaena* 7120 exposed to NaCl stress. J Plant Physiol 162:1030–1037. https://doi.org/10.1016/j.jplph.2004.11.002.
11. Wolf A, Krämer R, Morbach S. 2003. Three pathways for trehalose metabolism in *Corynebacterium glutamicum* ATCC13032 and their significance in response to osmotic stress. Mol Microbiol 49:1119–1134. https://doi.org/10.1046/j.1365-2958.2003.03625.x.
12. Saito K, Kase T, Takahashi E, Takahashi E, Horinouchi S. 1998. Purification and characterization of a trehalose synthase from the basidiomycete *Grifola frondosa*. Appl Environ Microbiol 64:4340–4345.
13. Goedl C, Schwarz A, Mueller M, Brecker L, Nidetzky B. 2008. Mechanistic differences among retaining disaccharide phosphorylases: insights from kinetic analysis of active site mutants of sucrose phosphorylase and α,α-trehalose phosphorylase. Carbohyd Res 343:2032–2040. https://doi.org/10.1016/j.carres.2008.01.029.
14. Wannet WJB, Op den Camp HJM, Wisselink HW, van der Drift C, Van Griensven LJLD, Vogels GD. 1998. Purification and characterization of trehalose phosphorylase from the commercial mushroom *Agaricus bisporus*. Biochim Biophys Acta 1425:177–188. https://doi.org/10.1016/S0304-4165(98)00066-X.
15. Goedl C, Griessler R, Schwarz A, Nidetzky B. 2006. Structure-function relationships for *Schizophyllum commune* trehalose phosphorylase and their implications for the catalytic mechanism of family GT-4 glycosyltransferases. Biochem J 397:491–500. https://doi.org/10.1042/BJ20060029.
16. Kizawa H, Miyagawa K, Sugiyama Y. 1995. Purification and characteriza-

tion of trehalose phosphorylase from *Micrococcus varians*. Biosci Biotech Bioch 59:1908–1912. https://doi.org/10.1271/bbb.59.1908.
17. Maruta K, Watanabe H, Nishimoto T, Kubota M, Chaen H, Fukuda S, Kurimoto M, Tsujisaka Y. 2006. Acceptor specificity of trehalose phosphorylase from *Thermoanaerobacter brockii*: production of novel nonreducing trisaccharide, 6-O-α-D-galactopyranosyl trehalose. J Biosci Bioeng 101:385–390. https://doi.org/10.1263/jbb.101.385.
18. Inoue Y, Ishii K, Tomita T, Yatake T, Fukui F. 2002. Characterization of trehalose phosphorylase from *Bacillus stearothermophilus* SK-1 and nucleotide sequence of the corresponding gene. Biosci Biotechnol Biochem 66:1835–1843. https://doi.org/10.1271/bbb.66.1835.
19. Van der Borght J, Chen C, Hoflack L, Van Renterghem L, Desmet T, Soetaert W. 2011. Enzymatic properties and substrate specificity of the trehalose phosphorylase from *Caldanaerobacter subterraneus*. Appl Environ Microbiol 77:6939–6944. https://doi.org/10.1128/AEM.05190-11.
20. Ryu S-I, Kim J-E, Huong NT, Woo E-J, Moon S-K, Lee S-B. 2010. Molecular cloning and characterization of trehalose synthase from *Thermotoga maritima* DSM3109: syntheses of trehalose disaccharide analogues and NDP-glucoses. Enzyme Microb Technol 47:249–256. https://doi.org/10.1016/j.enzmictec.2010.07.017.
21. Kouril T, Zaparty M, Marrero J, Brinkmann H, Siebers B. 2008. A novel trehalose synthesizing pathway in the hyperthermophilic crenarchaeon *Thermoproteus tenax*: the unidirectional TreT pathway. Arch Microbiol 190:355–369. https://doi.org/10.1007/s00203-008-0377-3.
22. Nobre A, Alarico S, Fernandes C, Empadinhas N, Da Costa MS. 2008. A unique combination of genetic systems for the synthesis of trehalose in *Rubrobacter xylanophilus*: properties of a rare actinobacterial TreT. J Bacteriol 190:7939–7946. https://doi.org/10.1128/JB.01055-08.
23. Woo E-J, Ryu S-I, Song H-N, Jung T-Y, Yeon S-M, Lee H-A, Park BC, Park K-H, Lee S-B. 2010. Structural insights on the new mechanism of trehalose synthesis by trehalose synthase TreT from *Pyrococcus horikoshii*. J Mol Biol 404:247–259. https://doi.org/10.1016/j.jmb.2010.09.056.
24. Ryu S-I, Kim J-E, Kim E-J, Chung S-K, Lee S-B. 2011. Catalytic reversibility of Pyrococcus horikoshii trehalose synthase: efficient synthesis of several nucleoside diphosphate glucoses with enzyme recycling. Process Biochem 46:128–134. https://doi.org/10.1016/j.procbio.2010.07.030.
25. Qu Q, Lee SJ, Boos W. 2004. TreT, a novel trehalose glycosyltransferring synthase of the hyperthermophilic archaeon *Thermococcus litoralis*. J Biol Chem 279:47890–47897. https://doi.org/10.1074/jbc.M404955200.
26. Tischler D, Niescher S, Kaschabek SR, Schlömann M. 2013. Trehalose phosphate synthases OtsA1 and OtsA2 of *Rhodococcus opacus* 1CP. FEMS Microbiol Lett 342:113–122. https://doi.org/10.1111/1574-6968.12096.
27. Lee SS, Hong SY, Errey JC, Izumi A, Davies GJ, Davis BG. 2011. Mechanistic evidence for a front-side, SN_i-type reaction in a retaining glycosyltransferase. Nat Chem Biol 7:631. https://doi.org/10.1038/nchembio.628.
28. Zaparty M, Hagemann A, Bräsen C, Hensel R, Lupas AN, Brinkmann H, Siebers B. 2013. The first prokaryotic trehalose synthase complex identified in the hyperthermophilic crenarchaeon *Thermoproteus tenax*. PLoS ONE 8:e61354. https://doi.org/10.1371/journal.pone.0061354.
29. Miao Y, Tenor JL, Toffaletti DL, Maskarinec SA, Liu J, Lee RE, Perfect JR, Brennan RG. 2017. Structural and *In vivo* studies on trehalose-6-phosphate synthase from pathogenic fungi provide insights into its catalytic mechanism, biological necessity, and potential for novel antifungal drug design. mBio 8:e00643-17. https://doi.org/10.1128/mBio.00643-17.
30. Cardoso FS, Castro RF, Borges N, Santos H. 2007. Biochemical and genetic characterization of the pathways for trehalose metabolism in *Propionibacterium freudenreichii*, and their role in stress response. Microbiology 153:270–280. https://doi.org/10.1099/mic.0.29262-0.
31. Cai X, Seitl I, Mu W, Zhang T, Stressler T, Fischer L, Jiang B. 2018. Biotechnical production of trehalose through the trehalose synthase pathway: current status and future prospects. Appl Microbiol Biotechnol 102:2965–2976. https://doi.org/10.1007/s00253-018-8814-y.
32. O'Neill MK, Piligian BF, Olson CD, Woodruff PJ, Swarts BM. 2017. Tailoring trehalose for biomedical and biotechnological applications. Pure Appl Chem 89:1223–1249. https://doi.org/10.1515/pac-2016-1025.
33. Nidetzky B, Gutmann A, Zhong C. 2018. Leloir glycosyltransferases as biocatalysts for chemical production. ACS Catal 8:6283–6300. https://doi.org/10.1021/acscatal.8b00710.
34. Urbanek BL, Wing DC, Haislop KS, Hamel CJ, Kalscheuer R, Woodruff PJ, Swarts BM. 2014. Chemoenzymatic synthesis of trehalose analogues: rapid access to chemical probes for investigating *Mycobacteria*. Chembiochem 15:2066–2070. https://doi.org/10.1002/cbic.201402288.
35. Yang Z, Zhang L, Zhang Y, Zhang T, Feng Y, Lu X, Lan W, Wang J, Wu H, Cao C, Wang X. 2011. Highly efficient production of soluble proteins from insoluble inclusion bodies by a two-step-denaturing and refolding method. PLoS One 6:e22981. https://doi.org/10.1371/journal.pone.0022981.
36. Sabogal A, Rio DC. 2010. A green fluorescent protein solubility screen in *E. coli* reveals domain boundaries of the GTP-binding domain in the P element transposase. Protein Sci 19:2210–2218. https://doi.org/10.1002/pro.499.
37. Davis SJ, Vierstra RD. 1998. Soluble, highly fluorescent variants of green fluorescent protein (GFP) for use in higher plants. Plant Mol Biol 36:521–528. https://doi.org/10.1023/A:1005991617182.
38. Coleman MA, Lao VH, Segelke BW, Beernink PT. 2004. High-throughput, fluorescence-based screening for soluble protein expression. J Proteome Res 3:1024–1032. https://doi.org/10.1021/pr049912g.
39. Su WW. 2005. Fluorescent proteins as tools to aid protein production. Microb Cell Fact 4:12. https://doi.org/10.1186/1475-2859-4-12.
40. Meints LM, Poston AW, Piligian BF, Olson CD, Badger KS, Woodruff PJ, Swarts BM. 2017. Rapid one-step enzymatic synthesis and all-aqueous purification of trehalose analogues. J Vis Exp 120:e54485. https://doi.org/10.3791/54485.
41. Lazaridis T, Lee I, Karplus M. 2008. Dynamics and unfolding pathways of a hyperthermophilic and a mesophilic rubredoxin. Protein Sci 6:2589–2605. https://doi.org/10.1002/pro.5560061211.
42. Trent JD. 1996. A review of acquired thermotolerance, heat-shock proteins, and molecular chaperones in archaea. FEMS Microbiol Rev 18:249–258. https://doi.org/10.1111/j.1574-6976.1996.tb00241.x.
43. Ditzel L, Löwe J, Stock D, Stetter K-O, Huber H, Huber R, Steinbacher S. 1998. Crystal structure of the thermosome, the archaeal chaperonin and homolog of CCT. Cell 93:125–138. https://doi.org/10.1016/S0092-8674(00)81152-6.
44. Kagawa HK, Yaoi T, Brocchieri L, McMillan RA, Alton T, Trent JD. 2003. The composition, structure and stability of a group II chaperonin are temperature regulated in a hyperthermophilic archaeon. Mol Microbiol 48:143–156. https://doi.org/10.1046/j.1365-2958.2003.03418.x.
45. Trent JD, Nimmesgern E, Wall JS, Hartl FU, Horwich AL. 1991. A molecular chaperone from a thermophilic archaebacterium is related to the eukaryotic protein t-complex polypeptide-1. Nature 354:490. https://doi.org/10.1038/354490a0.
46. Horwich AL, Willison KR. 1993. Protein folding in the cell: functions of two families of molecular chaperone, hsp 60 and TF55-TCP1. Philos Trans R Soc Lond B Biol Sci 339:313–326.
47. Marco S, Ureña D, Carrascosa JL, Waldmann T, Peters J, Hegerl R, Pfeifer G, Sack-Kongehl H, Baumeister W. 1994. The molecular chaperone TF55. FEBS Lett 341:152–155. https://doi.org/10.1016/0014-5793(94)80447-8.
48. Archibald JM, Logsdon JM, Doolittle WF. 1999. Recurrent paralogy in the evolution of archaeal chaperonins. Curr Biol 9:1053–1056. https://doi.org/10.1016/S0960-9822(99)80457-6.
49. Klumpp M, Baumeister W. 1998. The thermosome: archetype of group II chaperonins. FEBS Lett 430:73–77. https://doi.org/10.1016/S0014-5793(98)00541-9.
50. Scholz KE, Kopka B, Wirtz A, Pohl M, Jaeger K-E, Krauss U. 2013. Fusion of a flavin-based fluorescent protein to hydroxynitrile lyase from *Arabidopsis thaliana* improves enzyme stability. Appl Environ Microbiol 79:4727–4733. https://doi.org/10.1128/AEM.00795-13.
51. Shaner NC, Campbell RE, Steinbach PA, Giepmans BNG, Palmer AE, Tsien RY. 2004. Improved monomeric red, orange and yellow fluorescent proteins derived from *Discosoma* sp. red fluorescent protein. Nat Biotechnol 22:1567. https://doi.org/10.1038/nbt1037.
52. Jevševar S, Gaberc-Porekar V, Fonda I, Podobnik B, Grdadolnik J, Menart V. 2008. Production of nonclassical inclusion bodies from which correctly folded protein can be extracted. Biotechnol Progress 21:632–639. https://doi.org/10.1021/bp0497839.
53. García-Fruitós E, González-Montalbán N, Morell M, Vera A, Ferraz RM, Arís A, Ventura S, Villaverde A. 2005. Aggregation as bacterial inclusion bodies does not imply inactivation of enzymes and fluorescent proteins. Microb Cell Fact 4:27. https://doi.org/10.1186/1475-2859-4-27.
54. Seras-Franzoso J, Peternel S, Cano-Garrido O, Villaverde A, García-Fruitós E. 2015. Bacterial inclusion body purification. Methods Mol Biol 1258:293–305. https://doi.org/10.1007/978-1-4939-2205-5_16.
55. Diener M, Kopka B, Pohl M, Jaeger KE, Krauss U. 2016. Fusion of a coiled-coil domain facilitates the high-level production of catalytically active enzyme inclusion bodies. ChemCatChem 8:142–152. https://doi.org/10.1002/cctc.201501001.

56. Kloss R, Limberg MH, Mackfeld U, Hahn D, Grünberger A, Jäger VD, Krauss U, Oldiges M, Pohl M. 2018. Catalytically active inclusion bodies of L-lysine decarboxylase from E. coli for 1,5-diaminopentane production. Sci Rep 8:5856. https://doi.org/10.1038/s41598-018-24070-2.
57. Krauss U, Jäger VD, Diener M, Pohl M, Jaeger K-E. 2017. Catalytically-active inclusion bodies—carrier-free protein immobilizates for application in biotechnology and biomedicine. J Biotechnol 258:136–147. https://doi.org/10.1016/j.jbiotec.2017.04.033.
58. Huang K-P, Robinson JC. 1977. Effect of manganese(ous) and sulfate on activity of human placental glucose 6-phosphate-dependent form of glycogen synthase. J Biol Chem 252:3240–3244.
59. Murray BW, Takayama S, Schultz J, Wong C-H. 1996. Mechanism and specificity of human α-1,3-fucosyltransferase V. Biochemistry 35: 11183–11195. https://doi.org/10.1021/bi961065a.
60. Noor E, Haraldsdóttir HS, Milo R, Fleming RMT. 2013. Consistent estimation of Gibbs energy using component contributions. PLoS Comput Biol 9:e1003098. https://doi.org/10.1371/journal.pcbi.1003098.
61. Gutmann A, Krump C, Bungaruang L, Nidetzky B. 2014. A two-step O- to C-glycosidic bond rearrangement using complementary glycosyltransferase activities. Chem Commun (Camb) 50:5465–5468. https://doi.org/10.1039/c4cc00536h.
62. Gutmann A, Nidetzky B. 2016. Unlocking the potential of LeLoir glycosyltransferases for applied biocatalysis: efficient synthesis of uridine 5′-diphosphate-glucose by sucrose synthase. Adv Synth Catal 358: 3600–3609. https://doi.org/10.1002/adsc.201600754.
63. Fox JD, Waugh DS. 2003. Maltose-binding protein as a solubility enhancer. Methods Microbiol 205:99–117.
64. Kimple ME, Brill AL, Pasker RL. 2013. Overview of affinity tags for protein purification. Curr Protoc Protein Sci 73:Unit 9.9. https://doi.org/10.1002/0471140864.ps0909s73.
65. Žoldák G, Šuťák R, Antalík M, Sprinzl M, Sedlák E. 2003. Role of conformational flexibility for enzymatic activity in NADH oxidase from *Thermus thermophilus*. Eur J Biochem 270:4887–4897. https://doi.org/10.1046/j.1432-1033.2003.03889.x.
66. Gibson RP, Tarling CA, Roberts S, Withers SG, Davies GJ. 2004. The donor subsite of trehalose-6-phosphate synthase: binary complexes with UDP-glucose and UDP-2-deoxy-2-fluoro-glucose at 2 Å resolution. J Biol Chem 279:1950–1955. https://doi.org/10.1074/jbc.M307643200.
67. Studier FW. 2005. Protein production by auto-induction in high-density shaking cultures. Protein Expr Purif 41:207–234. https://doi.org/10.1016/j.pep.2005.01.016.
68. Singh A, Upadhyay V, Panda AK. 2015. Solubilization and refolding of inclusion body proteins. Methods Mol Biol 1258:283–291. https://doi.org/10.1007/978-1-4939-2205-5_15.

AMERICAN SOCIETY FOR MICROBIOLOGY | Applied and Environmental Microbiology®

AUTHOR CORRECTION

Correction for Mestrom et al., "Artificial Fusion of mCherry Enhances Trehalose Transferase Solubility and Stability"

Luuk Mestrom,[a] Stefan R. Marsden,[a] Marit Dieters,[a] Puck Achterberg,[a] Lysanne Stolk,[a] Isabel Bento,[b] Ulf Hanefeld,[a] Peter-Leon Hagedoorn[a]

[a]Biocatalysis, Department of Biotechnology, Delft University of Technology, Delft, The Netherlands
[b]EMBL Hamburg, Hamburg, Germany

Volume 85, issue 8, e03084-18, 2019, https://doi.org/10.1128/AEM.03084-18. The presented trehalose transferase from *Pyrobaculum yellowstonensis* fused to mCherry (mCherry-*Py*TreT) was mislabeled. The correct name for the given protein sequence fused to mCherry is trehalose transferase from *Thermoproteus uzoniensis* (mCherry-*Tu*TreT). The protein sequence was correct in all cases and only the name was incorrect throughout the article. This mistake did not alter the main conclusion of the article, i.e., that mCherry increases the solubility and stability of an aggregation-prone archaeal trehalose transferase. Hence, the presented results were obtained with mCherry-*Tu*TreT instead of mCherry-*Py*TreT.

Throughout the paper, all references to "mCherry-*Py*TreT" should be "mCherry-*Tu*TreT."

Page 1, Abstract, lines 9 and 10: "*Pyrobaculum yellowstonensis* (*Py*TreT)" should be "*Thermoproteus uzoniensis* (*Tu*TreT)."

Page 1, Importance, line 7: "*Pyrobaculum yellowstonensis*" should be "*Thermoproteus uzoniensis*."

Page 2, paragraph 4, line 1: "*Py*TreT" should be "*Tu*TreT."

Page 5, paragraph 1, lines 4 through 6: "Furthermore, a high intracellular concentration of 0.37 mg of trehalose per mg of protein was reported for *Pyrobaculum aerophilum* (1)...." should read "Furthermore, a high intracellular concentration of 0.10 mg of trehalose per mg of protein was reported for *Thermoproteus tenax* (1)...."

Page 5, paragraph 2, lines 1 and 2: "Due to the poor solubility of *Py*TreT, a fusion construct of mCherry and *Py*TreT..." should read "Due to the poor solubility of *Py*TreT, a fusion construct of mCherry and *Tu*TreT...."

Page 5, paragraph 2, lines 5 through 7: The following sentence should be deleted: "*Py*TreT has a pI similar to that of mCherry and was therefore chosen as a candidate for further investigations as the fusion construct mCherry-*Py*TreT."

Page 5, paragraph 4, line 9: "*Py*TreT" should be "mCherry-*Tu*TreT."

Page 6, paragraph 1, line 2: "*Py*TreT" should be "*Tu*TreT."

Page 6, paragraph 2, line 2: "*Py*TreT" should be "*Tu*TreT."

Page 6, paragraph 2, line 11: "$\varepsilon_{\text{mcherry-}Py\text{TreT}}$" should be "$\varepsilon_{\text{mcherry-}Tu\text{TreT}}$."

Page 9, paragraph 3, line 4: "*Py*TreT" should be "*Tu*TreT."

Page 10, paragraph 2, lines 5 and 7: "*Py*TreT" should be "*Tu*TreT."

Page 10, paragraph 3, line 1: "*Py*TreT" should be "*Tu*TreT."

Supplemental material: In Fig. S1, an additional SDS-PAGE of the produced N-terminal His_6-tagged *Tu*TreT protein (Fig. S1g) is given. This is referred to as Fig. S1g in the revised supplemental information. As well, throughout the supplemental material, "mCherry *Py*TreT" should be "mCherry *Tu*TreT." Revised supplemental material is posted online at https://doi.org/10.1128/AEM.03084-18.

Citation Mestrom L, Marsden SR, Dieters M, Achterberg P, Stolk L, Bento I, Hanefeld U, Hagedoorn P-L. 2019. Correction for Mestrom et al., "Artificial fusion of mCherry enhances trehalose transferase solubility and stability." Appl Environ Microbiol 85:e00942-19. https://doi.org/10.1128/AEM.00942-19.

Address correspondence to Peter-Leon Hagedoorn, P.L.Hagedoorn@tudelft.nl.

Published 1 July 2019